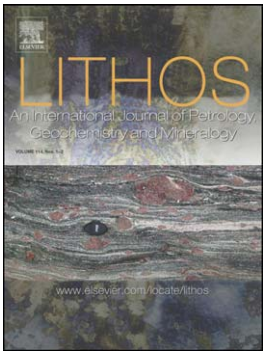

Origin and evolution of primitive melts from the Debunscha Maar, Cameroon: Consequences for mantle source heterogeneity within the Cameroon Volcanic Line

Caroline N. Ngwa, Thor H. Hansteen, Colin W. Devey, Froukje M. van der Zwan, Cheo E. Suh

PII: S0024-4937(17)30239-6
DOI: doi:10.1016/j.lithos.2017.06.028
Reference: LITHOS 4360

To appear in: *LITHOS*

Received date: 25 January 2017
Accepted date: 29 June 2017

Please cite this article as: Ngwa, Caroline N., Hansteen, Thor H., Devey, Colin W., van der Zwan, Froukje M., Suh, Cheo E., Origin and evolution of primitive melts from the Debunscha Maar, Cameroon: Consequences for mantle source heterogeneity within the Cameroon Volcanic Line, *LITHOS* (2017), doi:10.1016/j.lithos.2017.06.028

Origin and evolution of primitive melts from the Debunscha Maar, Cameroon: Consequences for mantle source heterogeneity within the Cameroon Volcanic Line.

Caroline N. Ngwa [a, b, c], Thor H. Hansteen[a*], Colin W. Devey[a], Froukje M. van der Zwan[a, d], Cheo E. Suh[b]

[a]GEOMAR Helmholtz Centre for Ocean Research Kiel, Wischhofstr. 1-3, D-24148 Kiel Germany

[d]Department of Geology, Faculty of Science, University of Buea, P. O box 63, SW Region Cameroon

[c]Mt. Cameroon Observatory, Institute for Geological and Mining Research, P.O box 370 Buea, SW Region Cameroon

[d]Institute of Geosciences, Christian Albrechts University Kiel, Ludewig-Meyn-Str.10, D-24118 Kiel, Germany

*corresponding author: thansteen@geomar.de

Abstract

Debunscha Maar is a monogenetic volcano forming part of the Mt. Cameroon volcanic field, located within the Cameroon Volcanic Line (CVL). Partly glassy cauliflower bombs have primitive basanite-picrobasalt compositions and contain abundant normally and reversely zoned olivine (Fo 77-87) and clinopyroxene phenocrysts. Naturally quenched melt inclusions in the most primitive olivine phenocrysts show compositions which, when corrected for post-entrapment modification, cover a wide range from basanite to alkali basalt (MgO 6.9-11.7wt.%), and are generally more primitive than the matrix glasses (MgO 5.0-5.5wt.%) and only partly fall on a common liquid line of descent with the bulk rock samples and matrix glasses. Melt inclusion trace element compositions lie on two distinct geochemical trends: one (towards high Ba/Nb) is thought to represent the effect of various proportions of anhydrous lherzolite and amphibole-bearing peridotite in the source, while the other (for example, high La/Y) reflects variable degrees of partial melting. Comparatively low fractionation-corrected CaO in the melt inclusions with the highest La/Y suggests minor involvement of a pyroxenite source component that is only visible at low degrees of melting. Most of the samples show elevated Gd/Yb,

indicating up to 8% garnet in the source. The range of major and trace elements represented by the melt inclusions covers the complete geochemical range given by basalts from different volcanoes of the Cameroon volcanic line, indicating that geochemical signatures that were previously thought to be volcano-specific in fact are probably present under all volcanoes. Clinopyroxene-melt barometry strongly indicates repeated mixing of compositionally diverse melts within the upper mantle at 830 ±170 MPa prior to eruption. Mantle potential temperatures estimated for the primitive melt inclusions suggest that the thermal influence of a mantle plume is not required to explain the magma petrogenesis.

Key words: Cameroon volcanic line, primitive melts, melts inclusions, Debunscha Maar

Abstract

Debunscha Maar is a monogenetic volcano forming part of the Mt. Cameroon volcanic field, located within the Cameroon Volcanic Line (CVL). Partly glassy cauliflower bombs have primitive basanite-picrobasalt compositions and contain abundant normally and reversely zoned olivine (Fo 77-87) and clinopyroxene phenocrysts. Naturally quenched melt inclusions in the most primitive olivine phenocrysts show compositions which, when corrected for post-entrapment modification, cover a wide range from basanite to alkali basalt (MgO 6.9-11.7wt.%), and are generally more primitive than the matrix glasses (MgO 5.0-5.5wt.%) and only partly fall on a common liquid line of descent with the bulk rock samples and matrix glasses. Melt inclusion trace element compositions lie on two distinct geochemical trends: one (towards high Ba/Nb) is thought to represent the effect of various proportions of anhydrous lherzolite and amphibole-bearing peridotite in the source, while the other (for example, high La/Y) reflects variable degrees of partial melting. Comparatively low fractionation-corrected CaO in the melt inclusions with the highest La/Y suggests minor involvement of a pyroxenite source component that is only visible at low degrees of melting. Most of the samples show elevated Gd/Yb, indicating up to 8% garnet in the source. The range of major and trace elements represented by the melt inclusions covers the complete geochemical range given by basalts from different volcanoes of the Cameroon volcanic line, indicating that geochemical signatures that were previously thought to be volcano-specific in fact are probably present under all volcanoes. Clinopyroxene-melt barometry strongly indicates repeated mixing of compositionally diverse melts within the upper mantle at 830 ±170 MPa prior to eruption. Mantle potential temperatures estimated for the primitive melt inclusions suggest that the thermal influence of a mantle plume is not required to explain the magma petrogenesis.

1. Introduction

The Cameroon Volcanic Line (CVL) is a 1600km-long line of volcanic centres which straddles the western margin of the African continent, extending from the island of Pagalu (2°S) in the Atlantic Ocean, across Cameroon and into the central part of Africa (Fig. 1). The oceanic sector is composed of six volcanoes, one each on Pagalu, Saõ Tomé and Principe Islands and three on Bioko Island (Deruelle et al., 2007). The continental sector contains some of the largest continental intraplate volcanoes on Earth interspersed with smaller edifices. The large volcanoes include Mt. Etinde, Mt. Cameroon, Mt. Manengouba, Mt. Bambouto, Mt. Oku, Ngaoundéré Plateau, Mandara Mts. and Bìu Plateau, while the smaller ones consist of cinders cones and maars, many un-named and unstudied.

The cause and mantle origins of the CVL melts are unclear: the volcanism shows no strong age progression (Fitton and Dunlop, 1985) arguing against the activity of a hotspot, although the magmas show chemical affinities to HIMU compositions (Ballentine et al., 1997; Halliday et al., 1990; Lee et al., 1994) a classical hotspot component. Several studies have attempted to address this problem (Dunlop, 1983; Fitton and Dunlop, 1985; Halliday et al., 1988a; Halliday et al., 1990; Tamen et al., 2007), but no unique conclusions have been reached. Alternative plume models have been proposed, e.g. Burke (2001) suggested interplay between a plume and the right-angled bend in the continental margin, Ngako et al. (2006) suggested that the CVL originates either from two mantle plumes acting in succession, or from lithospheric features that induce oblique alignments of magmatic complexes, Ebinger and Sleep (1998) suggested a magmatic connection to the Afar plume. However, in all cases an age progression would be expected. Based on work of Fitton (1980), the model of a hotline was proposed by several authors (Lee et al., 1994; Meyers et al., 1998). Déruelle et al. (2007) proposed that this hot line has an origin in a sub-lithospheric mantle involving depleted mantle and focal zone (FOZO) components. More recent models assume a physical cause for the CVL e.g. by mantle convection due to the edge convection adjacent to the cratons or due to lithosphere instabilities causing basal erosion of the lithosphere (Adams et al., 2015; De Plaen et al., 2014; Elsheikh et al., 2014; Milelli et al., 2012; Reusch et al., 2011), or shear zone reactivation, leading to ‘leaking’ of mantle-derived material through pre-exisisting lithospheric structures (Shellnut et al., 2016) and thus

assume an asthenospheric mantle source. Fitton and Dunlop (1985) and Fitton (1987) showed that the oceanic and continental rocks of the CVL have similar alkalic compositions. Halliday et al. (1988b) suggest an upwelling asthenospheric mantle as the source for these rocks but Sato et al. (1990) propose rather that the rocks have two sources, with those from polygenetic volcanoes originating from an upwelling asthenosphere beneath the African plate while those from the monogenetic volcanoes come from the lowest portion of the sub- continental lithosphere. Interaction between magmas from an asthenospheric source and a metasomatised amphibole bearing lithosphere was suggested for samples from the western highlands (Oku, Bambouto, Nyos) by e.g. Njilah et al. (2013) and Asaah et al. (2015b), while Kamgang et al. (2013) found also a pyroxenite component in some of the samples. Marzoli et al. (2000) suggested an asthenospheric and lithospheric source for samples from the western highlands and Mt. Cameroon, but a mere asthenospheric source for oceanic basalts and samples from Ngaoundéré. Samples from the ocean island Bioko, however, also show a metasomatic component that was interpreted as a mixture between asthenospheric melts and melts from the metasomatised (oceanic) lithosphere (Yamgouot et al., 2015).

Most geochemical studies have been centred on the large volcanoes and cinder cones. Despite the occurrence of many maars in the continental sector of the CVL, very few geochemical studies have been carried out on this type of volcano, even though maar volcanism, with its rapid phreatomagmatic quenching, deep origin and generally monogenetic nature, provides an ideal setting for geochemical source studies. In addition, studying the maars along the CVL is of high importance in terms of volcanic hazard assessment, as degassing of volcanic CO_2 from maars Nyos and Monoun caused the suffocation of >1700 people (Kling et al., 1987; Sigurdsson et al., 1987). In this paper, the compositions of whole-rock samples, matrix glasses, minerals and melt inclusions from cauliflower bombs collected from the Debunscha maar, which sits close to the ocean-continent boundary on the West African coast, west of Mount Cameroon, are presented and compared with published data from other CVL edifices. This is the first detailed geochemical and melt inclusion dataset for this type of volcano along the CVL and we use it to investigate the petrogenesis of the magmas and their mantle

source(s) and how they fit into the framework of the other volcanism along the continental sector of the CVL.

2. Sample location and analytical methods

Debunscha Maar (Fig. 1) is a monogenetic volcanic edifice, located on the West African coast at 04°06`09’’N and 08°58’45’’E. It rises to a maximum altitude of 65 m above sea level and is classified as forming part of the Mt. Cameroon volcanic field (Ngwa et al., 2010). The maar crater is filled with a fresh water lake. The inner walls of the crater rise steeply above the lake surface. Tephra deposits, covered with thick jungle, flanks the outer crater walls on all sides and decreases in thickness gently away from the crater area into the surrounding farmed area and into the sea. The physical volcanological attributes of this deposit have been described in detail by Ngwa et al. (2010).

Ten cauliflower bombs were collected from the tephra deposits. These bombs are fresh in hand specimen and measure up to 14 cm in diameter. Some have quenched and partly glassy surfaces, cracked and curved margins, and are largely non-vesicular.

Each bomb was cut into two portions; one portion from each pair was jaw-crushed and milled to fine powder for whole-rock geochemical analyses of major and trace element compositions. Polished thin sections were produced for optical microscopy and electron-microprobe analyses of matrix glasses, mineral phases and melt inclusions (MI). Furthermore, olivine phenocrysts were picked, mounted and polished for the detailed analysis of naturally quenched melt inclusions.

Major elements from bulk rocks were determined on fused beads using the Philips X- Unique PW1480 XRF spectrometer at GEOMAR Helmholtz-Zentrum für Ozeanforschung Kiel. Details of the analytical procedure and analytical accuracy and precision are given, for example, in Abratis (2002). Trace and rare earth elements (REE) were determined on an AGILENT 7500cs ICP-MS at the Geological Institute of the University of Kiel Germany, using methods as described in Garbe-Schönberg (1993). The international standards BHVO-2, BE-N and BCR and blanks were analysed as unknowns between samples for accuracy- and quality-control. The accuracy of the standard results

was generally within 0.1 - 9% of the working values. Precision (estimated from 5 replicate analyses of randomly selected samples) was generally better than ± 4%.

The major element contents of matrix glasses, minerals and melt inclusions were determined on a JEOL JXA-8200 Superprobe electron microprobe at GEOMAR using a 15 kV accelerating voltage. For each olivine and clinopyroxene phenocryst, both the core and the rim were analysed, with a minimum of two points per area. *Olivines* were analysed using a 100 nA current, a focussed beam and the San Carlos olivine (USNM 111312/44) as standard (Jarosewich, 2002). *Pyroxene* analyses were performed with a beam diameter of 1µm, 20nA current, and Kakanui Augite (USNM 122142) as a standard. *Matrix glasses and melt inclusions* were analysed using a beam diameter of 5µm, 10nA beam current and VGA 99 (USNM 113498/1) and VG-2 (USNM 111240) as standards.

To determine the original magmatic compositions of the melt inclusions, we used the method of Danyushevsky and Plechov (2011) by means of the program Petrolog3 and the model of Ford et al. (1983) to correct for post-entrapment crystallisation of olivine on the inclusion walls, and for consequent diffusive re-equilibration with the olivine host. Measured melt inclusion compositions were paired with host olivine compositions 10 to 20µm from the respective inclusions, considered to represent the original mineral compositions. Output of the calculations comprises corrected inclusion compositions in Fe-Mg equilibrium with the host grain, and presumed equilibration temperatures.

Trace elements in melt inclusions and matrix glasses were analysed by Laser-Ablation Inductively Coupled Plasma Mass Spectrometry at GEOMAR using a GeoLas Pro laser ablation system equipped with a 193 nm UV laser, coupled to a Nu Instruments AttoM single collector sector field ICP-MS (Fietzke and Frische, 2016). Analyses were performed using NIST610_11, ATHO, T1 and stHs6-80 standard reference materials (Jochum et al., 2006; Jochum et al., 2011) and their accuracy and precision are given in Table A.1. During analyses, laser spots were 16, 32 or 44µm depending on the size of the melt inclusions. For the largest inclusions, two spots were analysed on each inclusion and their compositions averaged.

3. Results

3.1. Petrography and mineral chemistry

The samples are all mildly porphyritic (~2-9% crystals) with olivine and clinopyroxene constituting the phenocrysts and microphenocrysts. The groundmass additionally comprises plagioclase microlites and fresh glass. The olivine and clinopyroxene phenocrysts are mostly euhedral to subhedral and range in size from 0.3-1.5mm. Glomerocrysts are rare. The microphenocrysts partly occur in aggregates, otherwise are isolated and completely or partly surrounded by fresh matrix glass. They are usually euhedral-subhedral and are smaller than 0.3mm. The measured melt inclusions in the minerals ranged in size from 30-150µm and are generally glassy, and sometimes contain shrinkage bubbles.

The forsterite (Fo) contents of olivine range from 77.8 to 86.9 mol% (Table A.2). The core compositions cluster in two groups; high magnesium cores (Fo 85-86.9 mol%), and low magnesium cores (Fo 77-78 mol%). The rim compositions range from Fo 81.0-86.3 mol%. Olivines with high magnesium cores show normal zoning, those with low magnesium cores show reverse zoning. Both olivine types occur in all samples. The CaO contents of all olivine phenocrysts are higher than 0.2wt.% (Table A.2; 3570 ppm mol Ca), in line with the magmatic origin of olivine in mafic rocks (Garcia et al., 1995; Hong et al., 2013; Ren et al., 2004). They are higher than those found for typical HIMU magmas (4000-5300 vs. 1600-3300 ppm; Weiss et al., 2016). Al and Mn contents in the olivines overlap with these HIMU lavas and range from 90-200 and 2500-5000 ppm respectively (Table A.2).

The clinopyroxene crystals are pale to yellowish green, brown or colourless in plane-polarized light. Although most crystals are euhedral to subhedral, a few clinopyroxene grains have serrated margins or rounded edges, and several show patchy (anhedral) cores or sieve textures, all suggestive of intermittent partial resorption. All clinopyroxene crystals fall in the range of diopside with Wo_{48} En_{47} Fs_{13} to Wo_{45} En_{39} Fs_{7} (Table A.3). Crystals within each of the samples show various zonation patterns, which are well seen in back-scattered electron (BSE) images (Fig. 2). A majority of the clinopyroxene crystals are normally zoned with higher Mg# (atomic Mg/(Mg+Fe)) in the cores than in the rims (Fig. 2, profile A-B). Some crystals are either unzoned or reversely zoned (Fig. 2, profile C-D), and others display compositional jumps typically related to resorption textures (Fig. 2, profile E-

F). Thus both olivine and clinopyroxene show normal and reversed zonation patterns and so comprise at least two compositional groups, pointing to multi-stage magma evolution at Debunscha Maar.

3.2. Whole rock and matrix glass major element compositions

Whole rock geochemical data for samples used in this study are given on Table A.4. Major element data show some compositional spread, with MgO values ranging from 8.9-12.5wt.%, CaO from 10.1-12.4wt% and SiO_2 from 43.8-47.3wt%. On the total alkalis vs. silica (TAS) classification diagram, the samples are basaltic and fall mostly in the alkali basalt field, although one picrobasalt and one basanite composition are present (Fig. 3).

The matrix glass is alkali-basaltic to trachybasaltic in composition (Fig. 3) and shows very narrow ranges in major elements, e.g. SiO_2 46.0-46.8wt.%, MgO 5.0-5.5wt.%, K_2O 1.1-1.2wt.% P_2O_5 0.4-0.5wt.% (Fig. 4). Microprobe analyses of matrix glasses are given in Table A.5. All the whole-rock samples show slight increases in incompatible major element concentrations with decreasing MgO contents towards the glass compositions (Fig. 4).

3.3. Major and minor element compositions of melt inclusions

The uncorrected MgO contents of melt inclusions in olivine range from 3.0-6.1wt.%. The corrected MgO contents (see "Analytical Methods") vary between 6.9 and 11.7wt.%, clearly higher than those of the matrix glasses (Fig. 4 and Table 1). Variations in major element compositions between the inclusions are considerably larger than those that may originate from post-entrapment inclusion zoning (e.g. Newcombe, et al. 2014), which thus appears to be of little or no importance. For all further considerations, we assume that the corrected inclusion compositions represent the melts initially trapped during growth of the respective olivine crystals. In the TAS diagram, the melt inclusions cover a range of compositions in the alkali basalt to tholeiite fields. They also show a much wider range in major element compositions at a given MgO than whole rocks and matrix glasses (e.g. Fig. 4). This compositional diversity is well illustrated by variations up to an order of magnitude for the incompatible elements P, Ti and K (see Fig. 4b) at a given MgO.

3.4. Trace element variations in whole rock samples and melt inclusions

The melt inclusions and whole-rock compositions show strong enrichment of the light over the heavy rare-earth element (LREE/HREE) and a maximum relative enrichment at Nb and Ta when plotted in a primitive-mantle-normalised multi-element diagram (Fig. 5). The trace elements show OIB-like patterns (Fig. 5), similar to those previously reported from the CVL (Asaah et al., 2015a; Kamgang et al., 2013; Marzoli et al., 2000; Suh et al., 2008; Yamgouot et al., 2015; Yokoyama et al., 2007).

The melt inclusions again show a wider range in all trace element compositions than the whole rocks. Some of the melt inclusions and all the whole rocks have a variably negative Pb anomaly. A negative Pb anomaly and an enrichment in Nb and Ta relative to Ba and Rb are a characteristic of HIMU magmas (Willbold and Stracke, 2006). The rare earth elements show $(La/Yb)_N$ ratios of 13 to 20 for whole rocks, whereas the inclusions show $(La/Yb)_N$ ratios of 6 to 23 with one outlier at 42. Compatible trace elements in the bulk rock samples fall into two groups with V and Sc showing negative correlations and others like Co, Cr and Ni showing positive correlations with MgO. Decreasing Ni and Cr with decreasing MgO (not shown) are in accordance with a control by fractionation of olivine and clinopyroxene from the melt.

4. Discussion

4.1. Magma differentiation processes

The matrix glasses of all samples show very homogeneous major-element compositions - this would appear at first glance to be consistent with the field evidence, which suggests that Debunscha Maar is monogenetic (Ngwa et al., 2010).

Most olivine and clinopyroxene phenocrysts are normally zoned, in line with their formation during fractional crystallization. Nevertheless, we see evidence for the involvement of at least two compositionally contrasting magmas in Debunscha petrogenesis: 1) a significant proportion of both olivine and clinopyroxene phenocrysts show reverse zonation; and 2) clinopyroxene grains often show textures suggestive of partial resorption or melting of the clinopyroxenes during earlier stages of magma evolution. Both features imply the coexistence and mixing of a comparatively primitive and a

more evolved component with different temperatures during early magma evolution, although whether these were two melts or a primitive magma and cumulates from an earlier, chemically similar magma batch is unclear. Such disequilibrium temperature conditions both during early magma evolution and ascent have previously been described in other systems by, for example, Annell et al. (2007); Browne and Gardner (2006); Feineman et al. (2010).

The larger compositional variations (especially in incompatible trace elements) seen between the whole rock analyses (Figs. 3, 4 & 5) can partly be attributed to variations in the proportion of olivine and clinopyroxene phenocrysts present in the individual bombs, as they broadly follow liquid lines of decent. Additional variation may reflect different melt compositions. This is also shown by the melt inclusions that cover a large range of chemical composition. If crystallization during ascent were the main process affecting magma evolution, the melt inclusion compositions should lie along liquid lines of descent (Cannatelli et al., 2007), showing systematic variations such as an increase of SiO_2 and incompatible elements with decreasing MgO, and a clear trend in melt inclusion compositions towards the matrix glasses. Debunscha melt inclusions show a range of compositions at a given MgO content (Fig. 4).

Thus the large range in incompatible trace element ratios of both melt inclusions and whole rocks cannot be explained by fractional crystallisation or accumulation processes alone and also support a mixed origin for the Debunscha magmas. We note that the melt inclusions are all more MgO-rich than the matrix glasses, consistent with their being comparatively primitive magmas. Olivine may crystallize and trap melt inclusions at almost any stage during ascent of mafic magmas and thus the inclusions may reflect the typical variations in melt chemistry during magma evolution and present in magma reservoirs.

4.2. Depth of magma stagnation

Chemical thermobarometry was used to constrain the conditions of crystallisation and melt inclusion formation and thus the depths of magma stagnation levels in the Debunscha system. Equilibrium temperatures between the melt inclusions and their host olivine were obtained using the Petrolog3 software of Danyushevsky and Plechov (2011) and the model of Ford et al. (1983), and fall

in the range 1153-1315 (±20) °C (Table 1). This overlaps well with the temperature range of 1099–1295 °C for primitive melt inclusions in olivine from recent Mount Cameroon magmas (Suh et al., 2008). A large compositional range in the melt inclusions at all equilibrium temperatures is a strong indication that compositionally variable melts were trapped over a wide range of temperatures.

Clinopyroxene rims in equilibrium with matrix glasses allowed for the computation of crystallization temperatures and pressures using the spreadsheet of Putirka (2008) and the formulations of Putirka et al. (1996). This method is suitable for a range of liquid compositions, and is well applicable to the basaltic Debunscha samples. The precision of the method for calculated T and *P* are ±30 °C and ±1.7 kbar, respectively, for individual mineral-melt pairs. In applying this method, we used the compositions of fresh matrix glass coexisting with clinopyroxene rims as the melt that was in equilibrium with the clinopyroxenes. An Fe^{2+}/Fe^{3+} ratio of 0.88 was used and equilibrium between clinopyroxene and its coexisting liquid was checked by comparing observed values of $K_D(Fe\text{-}Mg)^{cpx\text{-}liq}$ with the theoretical equilibrium value of 0.27±0.03. Samples with $K_D(Fe\text{-}Mg)^{cpx\text{-}liq}$ within this range yielded pressures and temperatures of 8.4kbar and 1133°C, 8.2kbar and 1132°C and 8.2kbar and 1148°C respectively. Assuming 3.3km per kbar (Putirka, 1999), such a pressure corresponds to a depth of 27±6 km. Interestingly, this overlaps with depth estimates for clinopyroxene-melt equilibration of the 1999 and 2000 AD eruptions of Mt. Cameroon (Geiger et al. 2016). This depth is probably just below the Moho beneath the Mt. Cameroon volcanic area, which has been estimated at 20km-22km (Ambeh et al., 1989). Using geophysical, petrological and geochemical data, Suh et al. (2003), concluded that primitive magmas from Mt. Cameroon come from the lithospheric mantle close to the crust-mantle boundary. Based on seismic data, Ateba et al. (2009) hypothesised the existence of a magma chamber at >20 km for Mt. Cameroon volcano. Our depth estimate for the Debunscha maar is consistent with this deep level of magma stagnation for the Mt. Cameroon region. This magma chamber must have existed long enough to allow for the growth of different populations of equilibrium olivine and clinopyroxene and the occurrence of magma mixing.

4.3. Source mineralogy

If we can account for effects of crystal fractionation and magma chamber processes on the evolution of Debunscha magmas, we can use their major and trace element compositions to make some statements about the mineralogy of their source. As the melt inclusions are all more MgO-rich than the matrix glass, and hence represent more primitive magmas, they experienced the lowest amounts of fractional crystallisation before being trapped. Melts from mantle pyroxenite sources will have lower fractionation-corrected CaO contents than those from peridotite sources (Herzberg, 2006; Walter, 1998). On a CaO versus MgO diagram (Fig. 6a) showing the fields of peridotite and pyroxenite partial melts after Herzberg and Asimow (2008), most of the Debunscha melt inclusions lie well within the peridotite field, although a subset having low CaO contents plots within the pyroxenite field (Fig. 6a). Although low Ca could be explained by clinopyroxene crystallisation and the Debunscha samples contain some clinopyroxene phenocrysts, the tendency for CaO to increase with decreasing MgO contents in all Debunscha samples suggests that it is not playing a significant petrogenetic role. For several of the melt inclusions that fall within the peridotite field in Fig 6a, we were able to calculate the primitive melt compositions using PRIMELT3, meaning that they only experienced olivine crystallisation (Herzberg and Asimow, 2015). Inclusions that could not be reproduced using PRIMELT3 were either influenced by pyroxene crystallisation/accumulation or may have a pyroxenite source (samples below the green line; Fig. 6a), or a carbonated peridotite source (U10MI01; Table A.6; Herzberg and Asimow, 2008). Thus most primitive melts fall within the peridotite field (Fig. 6a) and the last melts that were formed are in equilibrium with spinel peridotite (Table A.6; cf. Herzberg and Asimow, 2015), consistent with the clinopyroxene-melt pressure calculations. The olivine liquidus temperatures of these melts are 1270-1340°C and fall within the upper range of equilibrium temperatures calculated with Petrolog3. We interpret these results as evidence for a dominantly peridotitic source for the Debunscha magmas, and a lesser but significant influence of a pyroxenite source for some of the magma batches involved. Also in terms of the Mn/Fe ratios of their olivines, the Debunscha samples mostly overlap with (MORB) samples that have a peridotitic source, with little effect of a pyroxenite source, a characteristic shared with other HIMU lavas (Fig. 7; Weiss et al., 2016). Additionally, the olivines show high Ca/Al ratios, also overlapping

with the HIMU lavas from Weiss et al. (2016) that they interpreted to be a result of carbonatite metasomatism of a peridotitic sub-continental lithospheric mantle. This interpretation is consistent with the other evidence for a dominantly peridotitic mantle source for the Debunscha samples and with one of the inclusions that cannot be reproduced by PRIMELT as it shows a too high Ca/SiO_2 ratio, and thus points to a carbonated source (cf. Herzberg and Asimow, 2008).

The amount of melting and the amount of garnet involved in the mantle melting, which indicates the melting depth, can also be assessed by examining the variations in Gd/Yb and La/Yb ratios, as the light and heavy REE are fractionated to different extents during melting in the garnet stability field (Bogaard and Wörner, 2003; Yokoyama et al., 2007). The diagram in Fig. 8 is used to illustrate to what extent the observed spread in melt inclusion and whole-rock and glass compositions could be explained by comparing the data to a model of melting various degrees of a peridotite source with primitive mantle trace element contents and containing variable amounts of garnet (Yokoyama et al., 2007) as well as to a model of melting a metasomatised Gnt-Amph-lherzolite (Marzoli et al., 2000). Although some of our samples likely have a pyroxenite source rather than a lherzolite source, they will generally follow the same REE systematics, as the slope of the HREE will be controlled almost exclusively by residual garnet. Although the major elements show that the last melting occurred in the spinel stability field, most of the bulk-rock samples, glasses and melt inclusions have Gd/Yb ratios too high for melting to have occurred purely in the spinel lherzolite field (which produces negligible fractionation between Gd and Yb) and instead fall within the region of melts requiring a contribution from melting in the garnet peridotite field, thus indicating decompression melting from the garnet to the spinel stability field. Although the melt inclusions cover a wider geochemical range than either whole rocks or matrix glasses in Fig. 8, most results suggest that the total degrees of melting are <5% in the presence of up to 8% garnet in the source. This is the case for both the primitive mantle model as well as the metasomatised mantle model that includes amphibole (Fig. 8). These values are consistent with the melt fractions calculated by PRIMELT that are mostly <5%, with a few exceptions up to 11% melt. The low-Ca melt inclusions, which we suggested may be derived from a pyroxenite source, fall at the lower end of the range of partial melting (3% or lower).

In addition to variations in source mineralogy and depth and degree of partial melting, the trace element signatures of the Debunscha rocks and melt inclusions contain information on the source chemistry itself. Previous authors have suggested that a metasomatised, amphibole-bearing source may play a role in CVL petrogenesis, both due to the presence of amphibole-bearing xenoliths in some magmas and anomalies in Sr, Ba, P, Hf and Zr in further magmas (Déruelle et al., 2007; Kamgang et al., 2013; Marzoli et al., 2000; Yamgouot et al., 2015; Yokoyama et al., 2007). Fig. 9a illustrates this effect, plotting La/Y (as a proxy for slope of the REE pattern, related to degree of partial melting) against Ba/Nb (whose very similar mantle incompatibility means they will not be strongly affected by differences in degree of melting but can respond to specific source mineralogy, such as the presence of amphibole, which retains Ba). The variation visible in La/Y at almost constant Ba/Nb as seen in many of our inclusions is most likely related to variations in degree of melting, consistent with the spread in melt degrees we observe in Fig. 8. Within this group we see a relation to the major element chemistry of the melt inclusions - those inclusions with high La/Y (implying low degree of melting) are also those with the lowest CaO contents, which should result from preferential melting of a fusible pyroxenite component in the source. This may imply that the amount of pyroxenite present is low (<3%) and only visible in low amounts of melt, becoming diluted with higher amounts of melting. The spread in Ba/Nb can, however, not be explained by melting processes and requires varying sources. We assume that this reflects the presence of amphibole in the source, which would in turn point to the mantle having been metasomatised, a process which has previously been proposed for some volcanoes of the CVL based on their trace element and isotope systematics (Déruelle et al., 2007; Kamgang et al., 2013; Yokoyama et al., 2007). The amphibole signature is only present in the high-Ca samples, indicating that metasomatism affected only the peridotite-part of the mantle and is independent from the pyroxenite enrichment of the source. This is consistent with the olivine trace element data, which partly overlaps with the HIMU samples from Weiss et al. (2016) that indicate a carbonatite metasomatised peridotitic source, most likely the subcontinental lithospheric mantle (Fig. 9). The fact that the Debunscha samples show even higher Ca values than the HIMU samples may indicate a stronger metasomatic overprint of the lithosphere here.

In order to constrain the physical state of the mantle, we calculated the mantle potential temperatures of the melt inclusions, using PRIMELT3 (Herzberg and Asimow, 2015), which gives temperatures in the range of 1340-1405°C (Fig. 6b). These temperatures are similar to the 'ambient mantle temperatures' that are found for MORB, in contrast to the clearly higher temperatures that are found for other OIB samples that are believed to have formed from hotspots (Fig. 6b; Herzberg and Asimow, 2008). This means that we do not see any evidence for an anomalously hot mantle beneath the CVL, which renders it unlikely that Debunscha is related to a hotspot or hotline as suggested by e.g. Burke (2001) and Fitton (1980). Thus, models based on decompression melting would probably be more appropriate (e.g. (Adams et al., 2015; De Plaen et al., 2014; Elsheikh et al., 2014; Milelli et al., 2012; Reusch et al., 2011; Shellnut et al., 2016).

Summing up, the simplest model for the Debunscha magma plumbing system would be that melts produced at a variety of melting degrees of a (at least partially) metasomatised peridotite-dominated source containing amphibole and some pyroxenite with a normal mantle temperature, were pooled, mixed and partially crystallised in a sub-Moho magma chamber shortly before eruption. Such repeated magma mixing in the upper mantle is consistent with models for the magma feeding system of Mt. Cameroon itself (Fitton et al., 1983; Geiger et al., 2016).

4.4. Geochemistry of the Debunscha melts in the CVL context

When we compare the Debunscha melt inclusion data to literature data from the CVL, we see a general larger spread in melt and source composition than for individual volcanoes. For example, Yokoyama et al. (2007) estimated that 2-3% accumulated melts from a source containing <8% garnet are needed to produce the lavas from recent Mt. Cameroon eruptions, which is a significantly narrower range than estimated for some of the Debunscha melt inclusions. Narrower ranges have also been proposed for Lakes Nyos, Elum and Wum (<2% melt, with <6% garnet; Asaah et al. (2015a)), for Bioko (<3% melt, with 0-4% garnet; Yamgouot et al. (2015)) and for Mt. Oku and Mt. Bambouto (2-3%) and Ngaoundéré Plateau (1-2%; Marzoli et al. (2000)). However, the suggested melting range for Debunscha falls within that of comparatively primitive rocks along the continental sector of the CVL; for example in line with the results from picrobasalts and basanites of the Barombi Koto

volcanic fields which were estimated to require ≤ 8% melting of a garnet peridotite source (Tamen et al., 2007).

Regionally, we see on Fig. 9 that whole rock samples from individual volcanic centres tend to show either La/Y OR Ba/Nb variations but not both. For example, Mt Cameroon shows almost no Ba/Nb variation and a limited range of La/Y, as does the Ngaoundéré Plateau and Debunscha whole rocks. Other areas (e.g. Bambouto, Oku, Nyos) show Ba/Nb variations but almost no La/Y scatter. Only samples from the oceanic part of the CVL show both La/Y and Ba/Nb variations and these even extend outside the field formed by the continental CVL. This may indicate a slightly different source or melting processes for the oceanic CVL samples.

Considering the Debunscha melt inclusions in this regional setting, it appears that melts belonging to two distinct, regionally occurring geochemical trends were produced by the source of the Debunscha Maar, although the weighted average of these melts (which produced the erupted magmas) has a composition close to the "elbow" of the two trends. In other regions, either the source with residual amphibole dominated (such as at Nyos and Bambouto) or a peridotite source melted to varying, low degrees (as at Ngaoundéré plateau). A larger spread in individual melt compositions may still be present in the magma systems beneath these locations, but not visible in the whole rock measurements and undiscovered due to the lack of melt inclusion measurements.

Figure 9 also shows that the geochemical "lineage" of a particular volcano is not related to its volume - both the “big volcanoes” (Mt. Cameroon, Bambouto, Ngaoundéré) and the “monogenetic volcanoes” (Oku, Nyos, Debunscha) may be dominated by either of the geochemical trends, and their size differences do not appear to reflect derivation from different sources, as postulated by Sato et al. (1990). Neither are specific trends related to certain regions of the CVL, with Ba/Nb variations in erupted lavas found in multiple detailed studies all along the CVL. This also agrees with information from other geochemical tracers: Samples from both SW and NE of Debunscha (from the island of Bioko (Yamgouot et al., 2015) and the highlands (Bambouto-Bamenda-Oku; Kamgang et al 2013; Asaah et al 2015, Marzoli et al 2000)) have trace element patterns that indicate amphibole in the source, while U-systematics show that mantle metasomatism may also have occurred under Mt.

Cameroon (Yokoyama et al., 2007). Mantle xenoliths containing amphibole were found around Barombi Lake, Mt. Oku and the Ngaoundéré Plateau (Lee D-c, 1996; Prelević et al., 2013). Evidence for a pyroxenite source was found at Bamenda Mts. in the trace element patterns of the melts (Kamgang et al., 2013). Samples from the CVL are all characterised in their Pb-Nd-Sr isotopes by a mixed signal between depleted mantle, HIMU and an enriched mantle component (EM1) and generally interpreted by mixing of melts from an asthenospheric source interacting with a metasomatised lithosphere (Kamgang et al., 2013; Marzoli et al., 2000; Yamgouot et al., 2015). The Debunscha melt inclusion data confirm that different source compositions (pyroxenite and amphibole bearing peridotite) play a role, which means that at least one metasomatic component is ubiquitous underneath the CVL

5. Conclusions

The whole rock, mineral and melt inclusion compositions of samples of magmatic ejecta from Debunscha Maar, located on the Cameroon coast on the flanks of Mount Cameroon, were studied. Thermobarometry on clinopyroxene phenocrysts and crystal zoning shows that geochemically diverse melts were fractionally crystallised, mixed and collected in a magma chamber at upper mantle depths prior to formation of the Debunscha Maar. Nevertheless, both whole rock and melt inclusion data show that these processes alone cannot account for the range of magmatic compositions. Melting of a predominantly peridotitic source in the garnet stability field can explain most magmatic compositions - the involvement of a pyroxenitic and a metasomatic amphibole-bearing source component are implied for some low-Ca magmas and samples with high Ba/Nb ratios respectively. Regionally, the melt inclusions in Debunscha olivine phenocrysts cover almost the whole range of magmatic compositions seen along the entire 1600km long Cameroon Volcanic Line, implying that the source components involved at Debunscha are available under the rest of the Line.

Acknowledgements

This article was completed during visits to GEOMAR supported by a Schlumberger "Faculty for the Future" postdoctoral fellowship and a Deutsche Forschungsgemeinschaft/The World Academy of Sciences grant, both awarded to Caroline N. Ngwa. We thank Mario Thöner, Jan Fietzke, Matthias Frische, Dagmar Rau (all Geomar), Ulrike Westernströer and Dieter Garbe-Schönberg (both University Kiel) for analytical assistance. The comments of Godfrey Fitton, Greg Shellnutt and an anonymous reviewer greatly helped in improving the manuscript.

References

Abratis, M.S., H.-U.; Hansteen, T. H., 2002. Composition and evolution of submarine volcanic rocksfrom the central and western Canary Islands. International Journal of Earth Science (Geol Rundsch) 91, 562–582.

Adams, A.N., Wiens, D.A., Nyblade, A.A., Euler, G.G., Shore, P.J., Tibi, R., 2015. Lithospheric instability and the source of the Cameroon Volcanic Line: Evidence from Rayleigh wave phase velocity tomography. Journal of Geophysical Research: Solid Earth 120, 1708-1727.

Aka, F.T., Yokoyama, T., Kusakabe, M., Nakamura, E., Tanyileke, G., Ateba, B., Ngako, V., Nnange, J., Hell, J., 2008. U-series dating of Lake Nyos maar basalts, Cameroon (West Africa): Implications for potential hazards on the Lake Nyos dam. Journal of Volcanology and Geothermal Research 176, 212-224.

Ambeh, W., Fairhead, J., Francis, D., Nnange, J., Djallo, S., 1989. Seismicity of the Mount Cameroon region, west Africa. Journal of African Earth Sciences (and the Middle East) 9, 1-7.

Annell, H., Scoates, J.S., Weis, D., Giret, A., 2007. Petrology of flood basalts at the tholeiitic–alkalic transition and phenocryst compositions, mt. Marion Dufresne, Kerguelen Archipelago, Southern Indian Ocean. The Canadian Mineralogist 45, 809-835.

Asaah, A.N., Yokoyama, T., Aka, F.T., Usui, T., Kuritani, T., Wirmvem, M.J., Iwamori, H., Fozing, E.M., Tamen, J., Mofor, G.Z., 2015a. Geochemistry of lavas from maar-bearing volcanoes in the Oku Volcanic Group of the Cameroon Volcanic Line. Chemical Geology 406, 55-69.

Asaah, A.N.E., Yokoyama, T., Aka, F.T., Usui, T., Wirmvem, M.J., Tchamabe, B.C., Ohba, T., Tanyileke, G., Hell, J.V., 2015b. A comparative review of petrogenetic processes beneath the Cameroon Volcanic Line: Geochemical constraints. Geoscience Frontiers 6, 557-570.

Ateba, B., Dorbath, C., Dorbath, L., Ntepe, N., Frogneux, M., Delmond, J., Manguelle, D., 2009. Eruptive and earthquake activities related to the 2000 eruption of Mount Cameroon volcano (West Africa). Journal of Volcanology and Geothermal Research 179, 206-216.

Ballentine, C., Lee, D.-C., Halliday, A., 1997. Hafnium isotopic studies of the Cameroon line and new HIMU paradoxes. Chemical Geology 139, 111-124.

Bogaard, P., Wörner, G., 2003. Petrogenesis of basanitic to tholeiitic volcanic rocks from the Miocene Vogelsberg, Central Germany. Journal of Petrology 44, 569-602.

Browne, B.L., Gardner, J.E., 2006. The influence of magma ascent path on the texture, mineralogy, and formation of hornblende reaction rims. Earth and Planetary Science Letters 246, 161-176.

Burke, K., 2001. Origin of the Cameroon line of volcano- capped swells. The Journal of Geology 109, 349-362.

Cannatelli, C., Lima, A., Bodnar, R., De Vivo, B., Webster, J., Fedele, L., 2007. Geochemistry of melt inclusions from the Fondo Riccio and Minopoli 1 eruptions at Campi Flegrei (Italy). Chemical Geology 237, 418-432.

Danyushevsky, L.V., Plechov, P., 2011. Petrolog3: Integrated software for modeling crystallization processes. Geochemistry, Geophysics, Geosystems 12.

De Plaen, R., Bastow, I., Chambers, E., Keir, D., Gallacher, R., Keane, J., 2014. The development of magmatism along the Cameroon Volcanic Line: evidence from seismicity and seismic anisotropy. Journal of Geophysical Research: Solid Earth 119, 4233-4252.

Déruelle, B., Ngounouno, I., Demaiffe, D., 2007. The Cameroon Hot Line'(CHL): a unique example of active alkaline intraplate structure in both oceanic and continental lithospheres. Comptes Rendus Geoscience 339, 589-600.

Dunlop, H., 1983. Strontium isotope geochemistry and potassium-argon studies on volcanic rocks from the Cameroon Line, West Africa. University of Edinburgh.

Ebinger, C.J., Sleep, N., 1998. Cenozoic magmatism throughout east Africa resulting from impact of a single plume. Nature 395, 788-791.

Elsheikh, A.A., Gao, S.S., Liu, K.H., 2014. Formation of the Cameroon Volcanic Line by lithospheric basal erosion: Insight from mantle seismic anisotropy. Journal of African Earth Sciences 100, 96-108.

Feineman, M., Sruoga, P., Drew, D., Murray, T., 2010. Disequilibrium phenocryst textures in an Andean volcanic complex: mixing or rapid decompression?, AGU Fall Meeting Abstracts, p. 2389.

Fietzke, J., Frische, M., 2016. Experimental evaluation of elemental behavior during LA-ICP-MS: influences of plasma conditions and limits of plasma robustness. Journal of Analytical Atomic Spectrometry 31, 234-244.

Fitton, J., 1980. The Benue trough and Cameroon line—a migrating rift system in West Africa. Earth and Planetary Science Letters 51, 132-138.

Fitton, J., Kilburn, C., Thirlwall, M., Hughes, D., 1983. 1982 eruption of Mount Cameroon, west Africa. Nature 306, 327-332.

Fitton, J., 1987. The Cameroon line, West Africa: a comparison between oceanic and continental alkaline volcanism. Geological Society, London, Special Publications 30, 273-291.

Fitton, J., Dunlop, H., 1985. The Cameroon line, West Africa, and its bearing on the origin of oceanic and continental alkali basalt. Earth and Planetary Science Letters 72, 23-38.

Fitton, J.G., 2007. The OIB paradox. Geological Society of America Special Papers 430, 387-412.

Ford, C., Russell, D., Craven, J., Fisk, M., 1983. Olivine-liquid equilibria: temperature, pressure and composition dependence of the crystal/liquid cation partition coefficients for Mg, Fe2+, Ca and Mn. Journal of Petrology 24, 256-266.

Garbe- Schönberg, C.-D., 1993. Simultaneous determination of thirty-seven trace elements in twenty-eight international rocks standards by ICP- MS. Geostandards Newsletter 17, 81-97.

Garcia, M.O., Hulsebosch, T.P., Rhodes, J.M., 1995. Olivine- rich submarine basalts from the southwest rift zone of Mauna Loa Volcano: Implications for magmatic processes and geochemical evolution. Mauna Loa Revealed: Structure, Composition, History, and Hazards, 219-239.

Geiger, H., Barker, A.K., Troll, V.R., 2016. Locating the depth of magma supply for volcanic eruptions, insights from Mt. Cameroon. Scientific Reports 6.

Halliday, A., Dickin, A., Fallick, A., Fitton, J., 1988a. Mantle dynamics: a Nd, Sr, Pb and O isotopic study of the Cameroon line volcanic chain. Journal of Petrology 29, 181-211.

Halliday, A.N., Davidson, J.P., Holden, P., DeWolf, C., Lee, D.-C., Fitton, J.G., 1990. Trace-element fractionation in plumes and the origin of HIMU mantle beneath the Cameroon line. Nature 347, 523-528.

Herzberg, C., 2006. Petrology and thermal structure of the Hawaiian plume from Mauna Kea volcano. Nature 444, 605-609.

Herzberg, C., Asimow, P.D., 2008. Petrology of some oceanic island basalts: PRIMELT2. XLS software for primary magma calculation. Geochemistry, Geophysics, Geosystems 9.

Herzberg, C., Asimow, P., 2015. PRIMELT3 MEGA. XLSM software for primary magma calculation: Peridotite primary magma MgO contents from the liquidus to the solidus. Geochemistry Geophysics Geosystems 16, 563-578.

Hong, L.-B., Zhang, Y.-H., Qian, S.-P., Liu, J.-Q., Ren, Z.-Y., Xu, Y.-G., 2013. Constraints from melt inclusions and their host olivines on the petrogenesis of Oligocene-Early Miocene Xindian basalts, Chifeng area, North China Craton. Contributions to Mineralogy and Petrology 165, 305-326.

Jarosewich, E., 2002. Smithsonian microbeam standards. Journal of Research-National Institute of Standards and Technology 107, 681-686.

Jochum, K.P., Stoll, B., Herwig, K., Willbold, M., Hofmann, A.W., Amini, M., Aarburg, S., Abouchami, W., Hellebrand, E., Mocek, B., 2006. MPI- DING reference glasses for in situ microanalysis: New reference values for element concentrations and isotope ratios. Geochemistry, Geophysics, Geosystems 7.

Jochum, K.P., Weis, U., Stoll, B., Kuzmin, D., Yang, Q., Raczek, I., Jacob, D.E., Stracke, A., Birbaum, K., Frick, D.A., 2011. Determination of reference values for NIST SRM 610–617 glasses following ISO guidelines. Geostandards and Geoanalytical Research 35, 397-429.

Kamgang, P., Chazot, G., Njonfang, E., Ngongang, N.B.T., Tchoua, F.M., 2013. Mantle sources and magma evolution beneath the Cameroon Volcanic Line: geochemistry of mafic rocks from the Bamenda Mountains (NW Cameroon). Gondwana Research 24, 727-741.

Kling, G.W., Clark, M.A., WAGNER, G.N., COMPTON, H.R., HUMPHREY, A.M., DEVINE, J.D., EVANS, W.C., Lockwood, J.P., Tuttle, M.L., KOENIGSBERG, E.J., 1987. The 1986 lake nyos gas disaster in cameroon, west Africa. Science 236, 169-175.

Le Bas, M., Le Maitre, R., Streckeisen, A., Zanettin, B., 1986. A chemical classification of volcanic rocks based on the total alkali-silica diagram. Journal of Petrology 27, 745-750.

Lee D-c, H.A., Davies GR, Essene EJ, Fitton JG and Temdjim R 1996. Melt enrichment of shallow depleted mantle: a detailed petrological, trace element and isotopic study of mantle-derived xenoliths and megacrysts from the Cameroon Line. Jounal of Petrology 37, 415-441.

Lee, D.-C., Halliday, A.N., Fitton, J.G., Poli, G., 1994. Isotopic variations with distance and time in the volcanic islands of the Cameroon line: evidence for a mantle plume origin. Earth and Planetary Science Letters 123, 119-138.

Marzoli, A., Piccirillo, E., Renne, P., Bellieni, G., Iacumin, M., Nyobe, J., Tongwa, A., 2000. The Cameroon Volcanic Line revisited: petrogenesis of continental basaltic magmas from lithospheric and asthenospheric mantle sources. Journal of Petrology 41, 87-109.

Meyers, J.B., Rosendahl, B.R., Harrison, C.G., Ding, Z.-D., 1998. Deep-imaging seismic and gravity results from the offshore Cameroon Volcanic Line, and speculation of African hotlines. Tectonophysics 284, 31-63.

Milelli, L., Fourel, L., Jaupart, C., 2012. A lithospheric instability origin for the Cameroon Volcanic Line. Earth and Planetary Science Letters 335, 80-87.

Ngako, V., Njonfang, E., Nnange, J.M., 2006. The North–South Paleozoic to Quaternary trend of alkaline magmatism from Niger–Nigeria to Cameroon: Complex interaction between hotspots and Precambrian faults. Journal Of African Earth Sciences 45, 241-256.

Ngwa, C.N., Suh, C.E., Devey, C.W., 2010. Phreatomagmatic deposits and stratigraphic reconstruction at Debunscha Maar (Mt Cameroon volcano). Journal of Volcanology and Geothermal Research 192, 201-211.

Njilah, I.K., Amidou, M., Robert, T., Benjamin, N., 2013. Sr-Nd-Pb isotopic studies of lavas of Mt. Oku volcano, North West Cameroon: A case involving HIMU, depleted and enriched mantle sources. Journal of Geology and Mining Research 5, 124-135.

Prelević, D., Jacob, D.E., Foley, S.F., 2013. Recycling plus: a new recipe for the formation of Alpine–Himalayan orogenic mantle lithosphere. Earth and Planetary Science Letters 362, 187-197.

Putirka, K., 1999. Clinopyroxene+ liquid equilibria to 100 kbar and 2450 K. Contributions to Mineralogy and Petrology 135, 151-163.

Putirka, K., Johnson, M., Kinzler, R., Longhi, J., Walker, D., 1996. Thermobarometry of mafic igneous rocks based on clinopyroxene-liquid equilibria, 0–30 kbar. Contributions to Mineralogy and Petrology 123, 92-108.

Putirka, K.D., 2008. Thermometers and barometers for volcanic systems. Reviews in Mineralogy and Geochemistry 69, 61-120.

Ren, Z.-Y., Takahashi, E., Orihashi, Y., Johnson, K.T., 2004. Petrogenesis of tholeiitic lavas from the submarine Hana Ridge, Haleakala Volcano, Hawaii. Journal of Petrology 45, 2067-2099.

Reusch, A.M., Nyblade, A.A., Tibi, R., Wiens, D.A., Shore, P.J., Bekoa, A., Tabod, C.T., Nnange, J.M., 2011. Mantle transition zone thickness beneath Cameroon: evidence for an upper mantle origin for the Cameroon Volcanic Line. Geophysical Journal International 187, 1146-1150.

Sato, H., Aramaki, S., Kusakabe, M., Hirabayashi, J., Sano, Y., Nojiri, Y., Tchoua, F., 1990. Geochemical difference of basalts between polygenetic and monogenetic volcanoes in the central part of the Cameroon volcanic line. Geochemical Journal 24, 357-370.

Shellnutt, J., Lee, T.Y., Torng, P.K., Yang, C.C., Lee, Y.H., 2016. Late Cretaceous intraplate silicic volcanic rocks from the Lake Chad region: An extension of the Cameroon volcanic line? Geochemistry Geophysics Geosystems 17, 2803-2824.

Sigurdsson, H., Devine, J., Tchua, F., Presser, F., Pringle, M., Evans, W.C., 1987. Origin of the lethal gas burst from Lake Monoun, Cameroun. Journal of Volcanology and Geothermal Research 31, 1-16.

Suh, C., Ayonghe, S., Sparks, R., Annen, C., Fitton, J., Nana, R., Luckman, A., 2003. The 1999 and 2000 eruptions of Mount Cameroon: eruption behaviour and petrochemistry of lava. Bulletin of Volcanology 65, 267-281.

Suh, C., Luhr, J., Njome, M., 2008. Olivine-hosted glass inclusions from Scoriae erupted in 1954–2000 at Mount Cameroon volcano, West Africa. Journal of Volcanology and Geothermal Research 169, 1-33.

Tamen, J., Nkoumbou, C., Mouafo, L., Reusser, E., Tchoua, F.M., 2007. Petrology and geochemistry of monogenetic volcanoes of the Barombi Koto volcanic field (Kumba graben, Cameroon volcanic line): Implications for mantle source characteristics. Comptes Rendus Geoscience 339, 799-809.

Walter, M.J., 1998. Melting of garnet peridotite and the origin of komatiite and depleted lithosphere. Journal of Petrology 39, 29-60.

Weiss, Y., Class, C., Goldstein, S.L., Hanyu, T., 2016. Key new pieces of the HIMU puzzle from olivines and diamond inclusions. Nature 537, 666-670.

Willbold, M., Stracke, A., 2006. Trace element composition of mantle end- members: Implications for recycling of oceanic and upper and lower continental crust. Geochemistry, Geophysics, Geosystems 7.

Yamgouot, F.N., Déruelle, B., Mbowou, I.B.G., Ngounouno, I., Demaiffe, D., 2015. Geochemistry of the volcanic rocks from Bioko Island ("Cameroon Hot Line"): Evidence for plume-lithosphere interaction. Geoscience Frontiers.

Yokoyama, T., Aka, F.T., Kusakabe, M., Nakamura, E., 2007. Plume–lithosphere interaction beneath Mt. Cameroon volcano, West Africa: Constraints from 238U–230Th–226Ra and Sr–Nd–Pb isotope systematics. Geochimica et Cosmochimica Acta 71, 1835-1854.

List of Figures

Fig. 1. Distribution of prominent volcanic complexes and selected maars within the Cameroon volcanic line (CVL). The Debunscha maar (in red box) is located on the lower southwestern flank of Mt. Cameroon Volcano, and thus close to the ocean- continent boundary of the CVL. Radiometric ages indicated in parentheses are from (Suh et al., 2008)

Fig. 2. Textures and zonation patterns of typical clinopyroxene phenocrysts as observed in back-scattered electron images. The white lines indicate the positions of the compositional profiles. **a** Normal zoning pattern, **b** Reversely zoned crystal comprising a low-magnesium core, **c** Pyroxene with low-magnesium core followed by a sharp increase in Mg# and a steep normal zonation toward the rim.

Fig. 3. Compositions of whole-rock samples, matrix glasses and melt inclusions in olivine from Debunscha Maar shown in a section of the total alkali vs. silica diagram (Le Bas et al., 1986). Melt inclusion compositions were corrected for post-entrapment crystallization and diffusive re-equilibration as detailed in the main text.

Fig. 4. Major element vs. MgO variation diagrams of whole-rock samples, corrected melt inclusions and matrix glasses. Literature data for Etinde and Mt. Cameroon (Fitton, 2007) are included for comparison together with fields for oceanic and continental samples from the CVL.

Figs. 5. Primitive mantle-normalized multi-element diagrams for the whole-rock and melt inclusions from the Debunscha maar. Fields for samples from the oceanic and continental CVL are given for comparison based on data from Asaah et al. (2015a); Kamgang et al. (2013); Marzoli et al. (2000); Suh et al. (2008); Yamgouot et al. (2015).

Fig. 6. MgO and CaO contents of Debunscha samples representing compositions of the corrected melt inclusions and primitive melts calculated by PRIMELT. Bulk rocks and glasses are shown for comparison. Blue lines define upper and lower CaO filters of primary magmas of fertile peridotite produced by accumulated fractional melting and is defined by the equation CaO= 1,095+0,154MgO +116,58/MgO. Green line defined by Ca= -0,274MgO +13,81 separates potential peridotite melts

above from pyroxenite melts below. Peridotite and pyroxenite lines are from Herzberg and Asimov (2015). Note that the melt inclusions data fall both in the pyroxenite (below green line) and peridotite source regions (above green line).

Fig. 7. Olivine Ca/Al against 100Mn/Fe ratios compared to olivines from HIMU, MORB, Iceland and Hawaiian basalts from Weiss et al. (2016). The Debunscha samples partially overlap with the HIMU data but with higher Ca/Al contents.

Fig. 8. Possible variations in source compositions and degrees of melting for the Debunscha samples, depicted in a Gd/Yb versus La/Yb diagram. Broken and solid curves are from Yokoyama et al. (2007) and represent percentages of melting and garnet in a peridotite source respectively. Dotted curve is from Marzoli et al. (2000)and shows the 0-10% melting curve of a garnet-amphibole lherzolite.

Fig. 9. Comparison of trace element data from Debunscha melt inclusions, bulk rocks and glasses to literature whole rock data from Mt. Cameroon, Bambouto mountains, Mt. Oku, Ngaoundéré plateau, Lake Nyos and a field for oceanic CVL (Aka et al., 2008; Fitton, 2007; Marzoli et al., 2000; Sato et al., 1990; Suh et al., 2008; Tamen et al., 2007). Inset for clarity, shows only data from the present study.

Appendix List

Table A.1: Precision and accuracy of standards used for LA-ICP-MS

Table A.2: Microprobe analyses of olivine phenocrysts from Debunscha

Table A.3: Chemical analyses of clinopyroxene phenocrysts from Debunscha

Table A.4: Whole rock geochemical data from Debunscha samples. Major elements are given in wt.% and trace elements in ppm.

Table A.5: Microprobe analyses of Matrix glasses from Debunscha

Table A.6: Primitive melt compositions calculated by PRIMELT

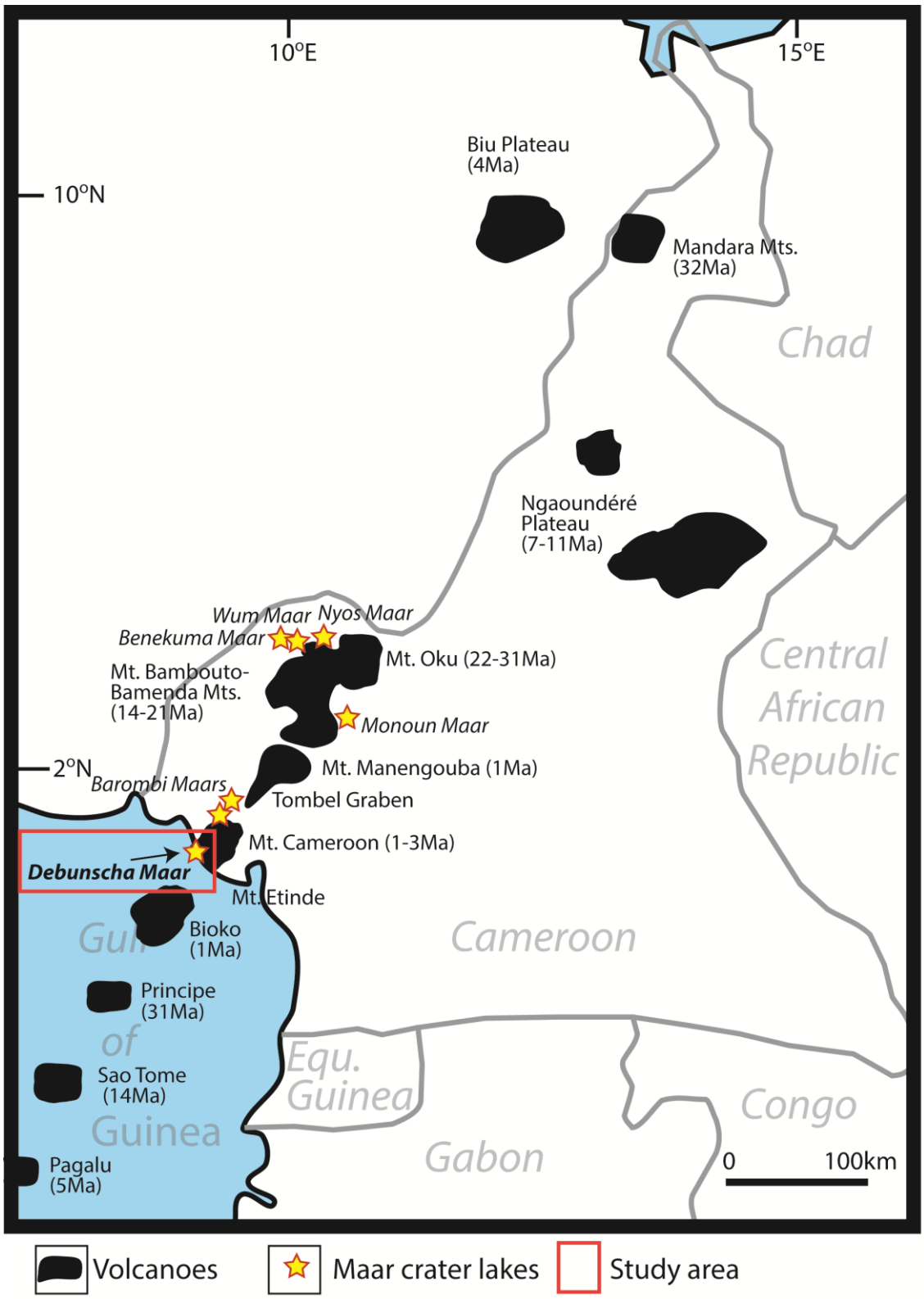

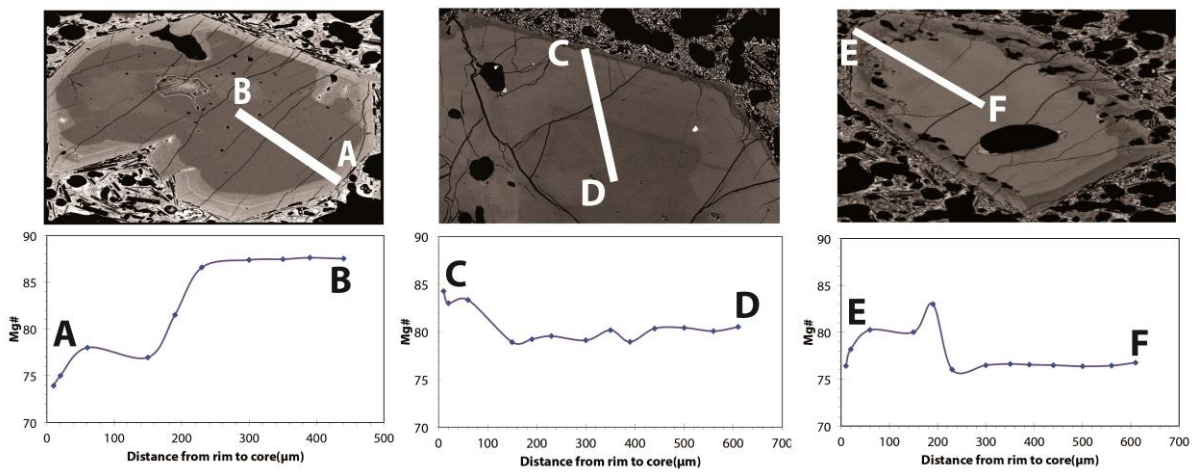

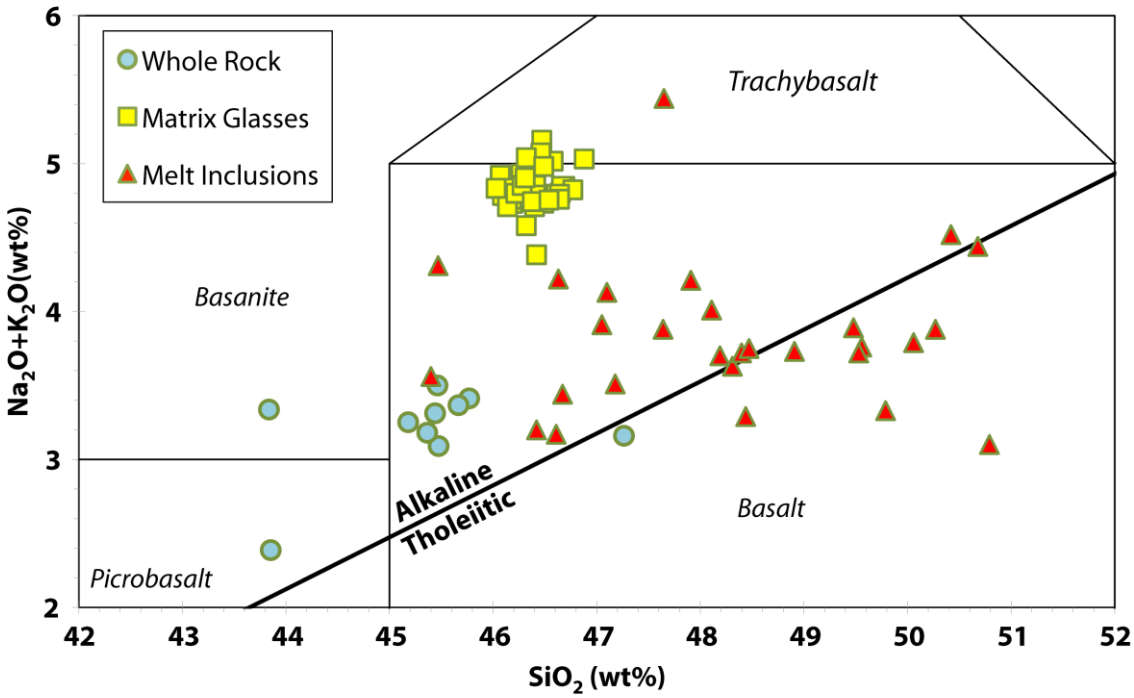

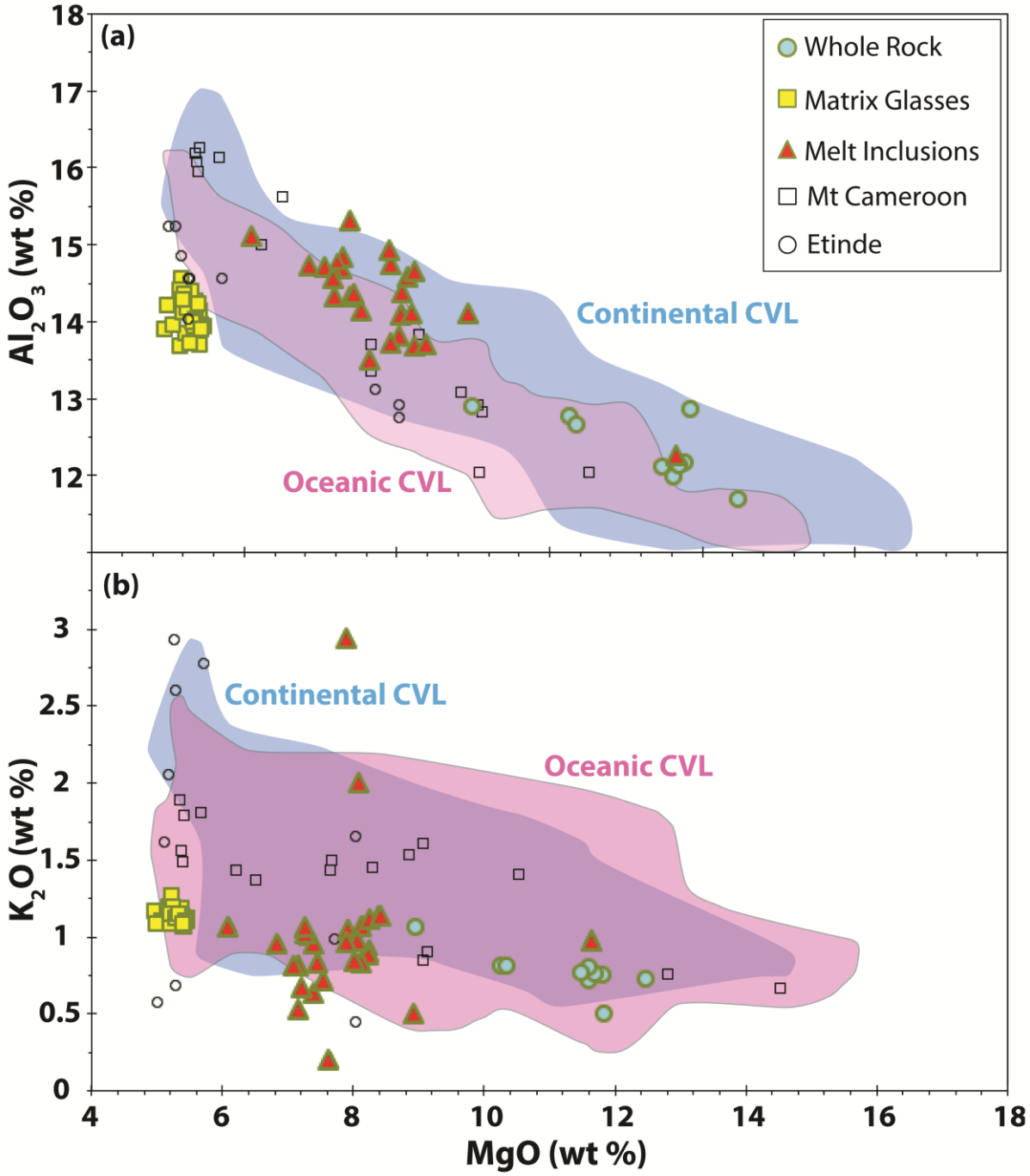

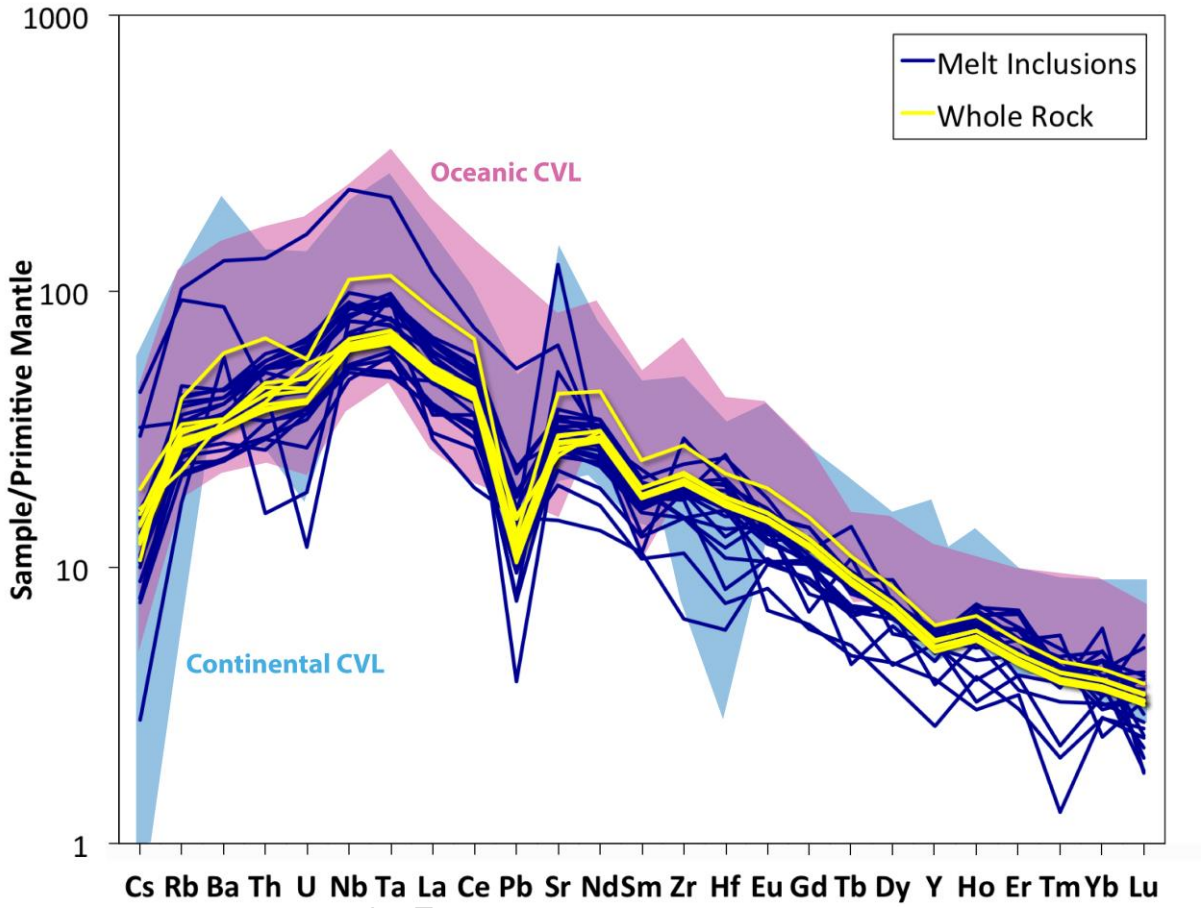

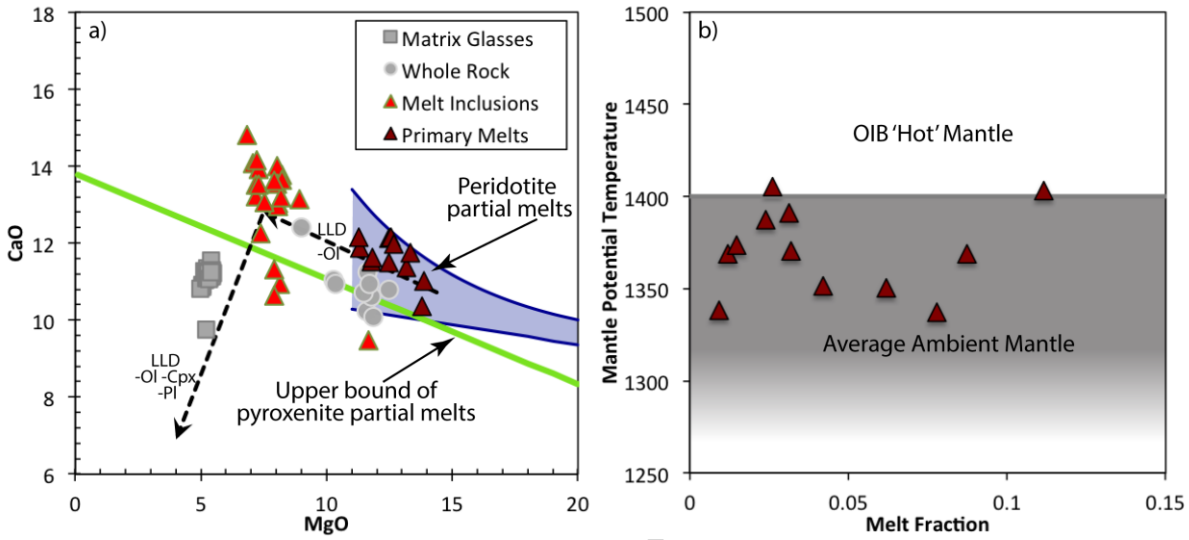

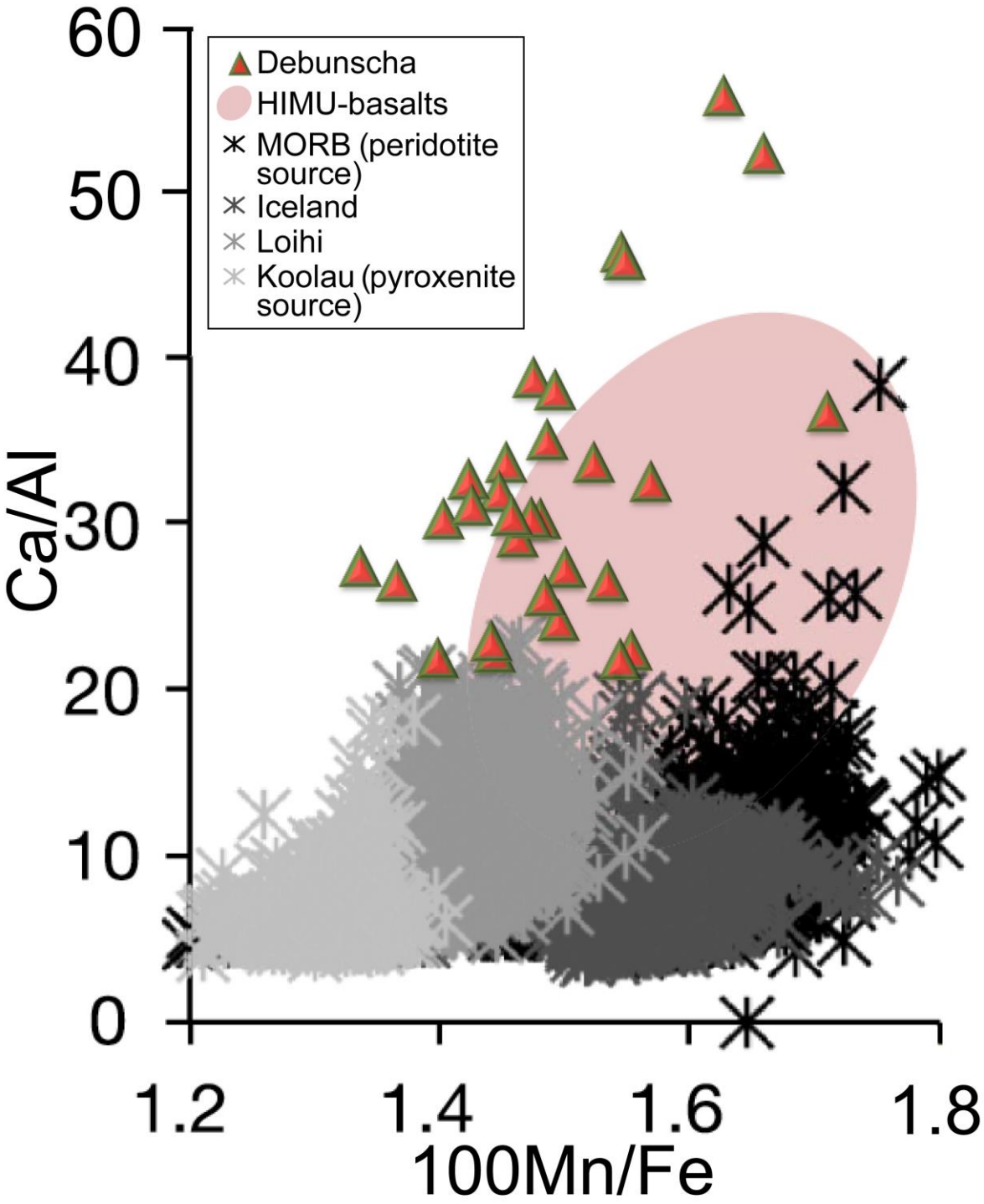

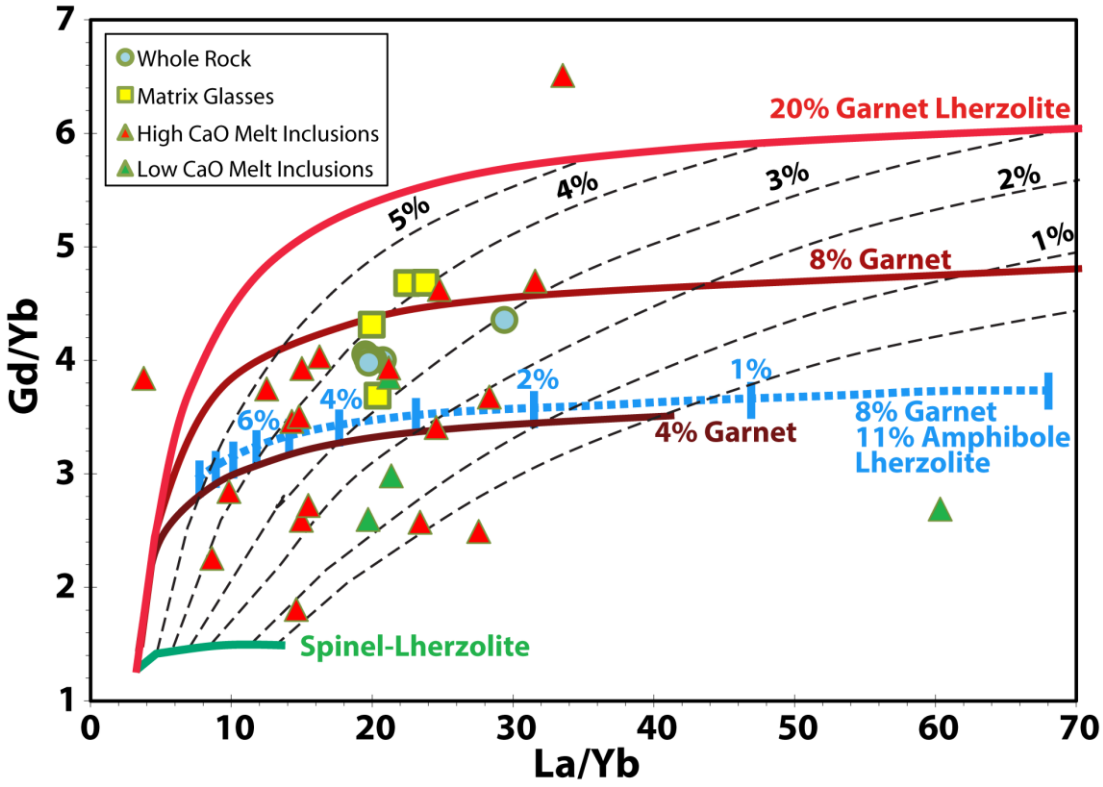

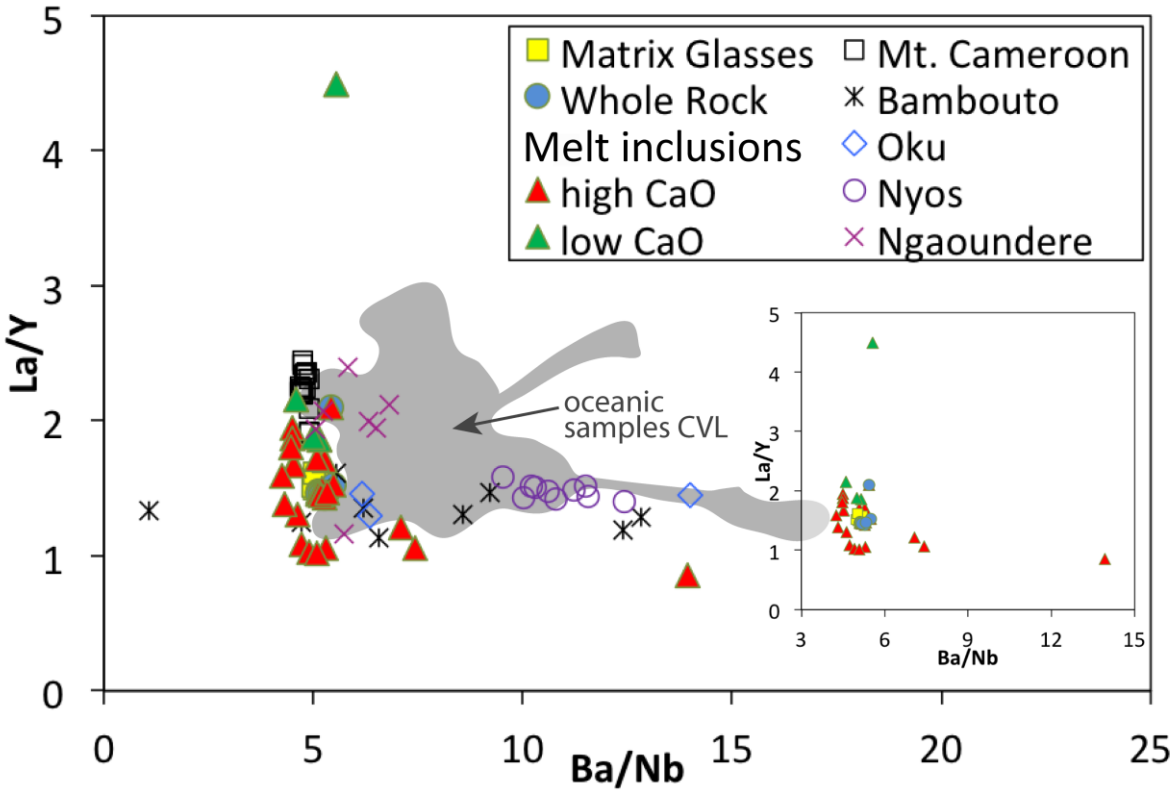

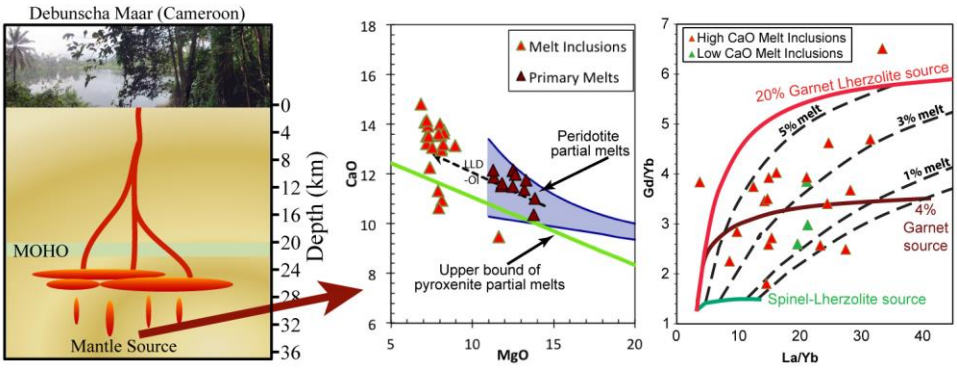

Table 1 - Major and trace element analyses of melt inclusions from Debunscha samples

Sample	U10MI01	U10MI03	U10MI04	U10MI05	*U10MI01-1*[a]	U8MMI01	U8mMI02	U8MMI03	*U5MI01*[a]	U5MI 02	U5MI03
Major elements (wt%)											
SiO2	45.4	48.2	46.6	49.5	*50.3*	47.1	47.2	48.9	*50.7*	48.3	47.7
TiO2	4.8	3.1	3.8	3.1	*2.9*	3.2	2.9	2.9	*2.6*	2.8	2.7
Al2O3	13.7	14.1	14.4	14.3	*14.6*	14.7	13.8	14.7	*14.8*	14.1	14.9
FeO	10.13	9.29	9.04	8.35	*8.81*	8.9	10.15	8.11	*8.69*	9.16	9.17
MnO	0.1	0.1	2.2	0.1	*0.1*	0.1	0.2	0.1	*0.1*	0.1	0.1
MgO	8.24	8.07	8.07	7.19	*8.14*	6.85	8.02	7.06	*7.92*	8.04	7.90
CaO	13.8	13.0	13.0	13.2	*10.9*	14.8	14.0	14.1	*10.7*	13.5	11.3
Na2O	2.4	2.9	2.2	3.2	*2.8*	3.0	2.7	2.9	*3.4*	2.6	2.5
K2O	1.1	0.8	2.0	0.7	*1.1*	1.0	0.8	0.8	*1.1*	1.0	2.9
P2O5	0.29	0.36	0.74	0.31	*0.32*	0.36	0.29	0.38	*0.09*	0.29	0.80
Trace elements (ppm)											
Li	4.98	5.18	5.20	2.57	*3.80*	5.00	5.29	4.29	*3.26*	3.19	3.89
Sc	36.0	28.2	32.5	30.3	*17.2*	31.7	33.2	30.1	*22.6*	28.6	27.2
V	393.1	285.9	405.0	274.4	*168.5*	368.3	366.2	300.3	*201.2*	293.2	365.8
Cr	150.8	207.0	167.4	272.7	*250.2*	163.4	123.8	192.7	*179.1*	209.8	113.1
Co	39.7	54.6	39.2	36.6	*149.7*	32.9	37.7	35.7	*113.2*	49.6	34.3
Ni	131.4	318.6	89.5	112.7	*1414.5*	45.9	59.2	84.6	*908.5*	259.6	95.3
Cu	103.5	114.0	61.3	87.3	*37.1*	65.9	102.5	101.4	*11.4*	60.8	53.6
Zn	107.4	137.5	124.1	98.4	*162.6*	98.9	130.6	92.4	*151.7*	107.1	116.6
Ga	28.9	26.4	36.5	23.7	*16.8*	27.5	26.7	24.4	*21.4*	25.7	40.5
Ge	1.65	1.65	1.62	b.d.l.	*1.92*	1.73	2.30	1.40	*0.96*	b.d.l.	2.42
Rb	10.3	18.5	55.7	13.2	*14.3*	18.8	19.6	15.9	*16.9*	22.9	61.0
Sr	1016.4	565.5	295.0	502.6	*394.0*	624.6	560.7	540.6	*531.6*	583.9	1266.0
Y	21.7	24.9	22.1	22.0	*11.4*	22.5	20.9	24.0	*16.1*	22.6	16.9
Zr	159.7	197.5	68.3	201.6	*118.4*	201.2	194.7	194.3	*158.5*	184.0	308.4
Nb	51.5	45.6	41.6	34.5	*34.9*	52.6	45.5	35.1	*45.1*	51.4	153.7
Mo	b.d.l.	3.47	6.18	4.24	*b.d.l.*	2.60	2.13	2.33	*2.82*	b.d.l.	5.63
In	0.10	0.10	0.11	0.09	*0.10*	0.12	0.10	0.05	*b.d.l.*	b.d.l.	0.07
Sn	1.65	2.37	0.82	2.02	*0.90*	1.65	1.90	1.91	*1.77*	1.41	1.65
Cs	0.06	0.34	0.90	b.d.l.	*0.19*	0.16	0.23	0.28	*b.d.l.*	b.d.l.	0.63
Ba	382.0	210.8	579.0	163.1	*160.5*	238.0	236.5	186.0	*232.1*	271.2	853.9
La	23.1	32.7	18.9	24.0	*24.7*	37.7	31.4	25.4	*30.0*	38.7	75.9
Ce	59.8	75.0	32.6	54.9	*49.4*	76.0	70.3	52.8	*66.5*	85.4	123.0
Pr	8.54	8.35	3.94	7.17	*5.89*	9.65	8.12	7.16	*7.41*	9.30	11.31
Nd	37.2	36.7	17.0	29.9	*20.9*	38.7	33.1	30.8	*29.1*	34.3	33.7
Sm	7.83	5.37	4.61	6.68	*4.36*	7.84	6.87	6.93	*6.43*	7.23	4.55
Eu	2.16	1.95	1.58	2.27	*1.29*	2.03	2.47	2.37	*1.60*	1.65	1.08
Gd	5.59	5.66	4.96	5.68	*3.25*	6.85	5.52	7.60	*5.57*	4.78	3.38
Tb	0.87	0.85	0.68	0.69	*0.51*	0.82	0.66	0.90	*0.72*	0.66	0.47
Dy	4.84	5.08	4.92	4.39	*2.52*	4.90	4.96	4.78	*4.67*	2.99	3.05
Ho	0.86	0.81	0.94	0.69	*0.60*	0.82	1.03	1.10	*0.79*	0.58	0.45
Er	2.20	2.08	2.58	2.11	*1.35*	2.65	1.97	2.65	*1.57*	2.10	1.51
Tm	0.26	0.32	0.27	0.29	*0.14*	0.35	0.27	0.29	*0.22*	0.25	0.09
Yb	1.61	2.18	2.20	1.62	*1.25*	1.78	2.03	2.03	*1.42*	2.65	1.26
Lu	0.24	0.23	0.20	0.15	*0.18*	0.28	0.17	0.27	*0.19*	0.12	0.16
Hf	3.91	4.93	1.67	5.36	*2.10*	4.96	3.64	4.32	*4.55*	2.36	5.67
Ta	2.80	2.69	3.49	1.90	*1.83*	3.51	2.56	2.10	*2.31*	2.77	8.08
W	0.24	0.38	2.06	0.54	*0.15*	0.58	0.55	1.40	*1.12*	0.83	1.65
Tl	0.05	0.08	0.05	b.d.l.	*b.d.l.*	b.d.l.	0.06	0.04	*b.d.l.*	0.15	0.18
Pb	1.18	3.51	2.27	2.31	*1.84*	2.47	2.15	1.43	*1.14*	0.58	7.86
Th	1.25	3.46	3.52	2.32	*2.65*	3.72	3.15	2.11	*3.31*	4.18	10.43
U	0.38	1.02	0.24	0.77	*0.76*	1.16	0.92	0.74	*0.95*	1.11	3.26
T (°C) [b]	1203	1153	1203	*1176*	1215	1154	1163	*1165*	1219	1198	1217

Table 1 continued

Sample	H7MI01	H7MI01-1	S2tp01	s2tp02	H4MI01	H4MI02	S2m-MI02	U3MI02	U3MI01	*U2MI01* [a]	U2MI03
Major elements (wt%)											
SiO2	48.4	50.8	47.1	47.9	49.6	46.4	45.5	48.4	47.6	*49.8*	48.5
TiO2	2.8	2.6	2.9	2.9	3.1	3.6	3.0	2.5	3.1	*3.0*	3.0
Al2O3	14.7	14.7	14.8	14.8	14.3	14.1	12.3	14.7	14.1	*14.2*	13.7
FeO	8.76	7.85	8.65	8.38	9.12	10.25	13.29	8.69	9.43	*8.6*	9.03
MnO	0.1	0.1	0.1	0.2	0.2	0.2	0.2	0.1	0.1	*0.2*	0.2
MgO	7.28	7.18	7.29	7.21	7.38	8.94	11.65	8.24	8.20	*7.54*	7.92
CaO	13.9	13.5	13.5	14.1	12.3	13.1	9.5	13.6	13.2	*13.1*	13.6
Na2O	2.7	2.6	3.1	3.2	3.1	2.7	3.3	2.4	3.0	*2.6*	2.8
K2O	1.0	0.5	1.1	1.0	0.6	0.5	1.0	0.9	0.9	*0.7*	1.0
P2O5	0.34	0.11	0.35	0.33	0.35	0.17	0.38	0.44	0.35	*0.32*	0.33
Trace elements (ppm)											
Li	5.33	7.91	5.53	4.55	5.19	4.48	4.43	4.46	5.12	*4.89*	5.49
Sc	33.3	40.0	34.3	32.9	35.7	40.0	29.7	31.9	31.0	*24.8*	31.5
V	319.3	376.2	315.6	329.0	292.4	430.7	268.4	302.9	299.3	*227.1*	285.4
Cr	199.0	198.2	167.2	171.4	178.5	197.6	163.2	143.1	146.9	*157.2*	106.8
Co	32.8	34.5	34.1	32.8	36.4	42.5	30.4	38.7	43.4	*89.2*	56.4
Ni	67.0	77.5	67.8	71.1	61.0	93.2	80.5	150.8	190.2	*673.3*	361.6
Cu	112.5	105.2	74.0	41.3	106.3	92.9	28.6	84.4	123.0	*85.5*	47.1
Zn	105.8	141.4	106.8	114.9	110.2	144.6	95.4	99.3	87.7	*139.4*	97.6
Ga	25.3	26.9	26.8	26.1	23.0	26.8	24.5	26.8	26.6	*17.7*	28.6
Ge	2.34	1.40	1.76	2.31	1.33	1.43	1.39	1.26	2.01	*b.d.l.*	3.60
Rb	21.4	15.0	24.7	23.7	15.1	13.6	25.3	27.2	20.4	*12.9*	20.1
Sr	645.1	743.3	699.2	672.5	549.5	2481.9	677.3	699.9	607.1	*445.5*	633.2
Y	21.6	24.0	23.5	25.6	23.6	25.2	22.8	23.1	22.6	*19.6*	23.0
Zr	197.1	249.1	215.7	199.6	212.6	158.1	198.5	207.0	186.1	*157.9*	191.5
Nb	57.4	46.7	64.8	60.0	35.7	33.4	58.0	56.8	54.2	*31.4*	57.7
Mo	3.16	4.81	2.97	1.57	2.03	b.d.l.	2.05	2.65	2.83	*2.79*	11.26
In	0.11	b.d.l.	0.09	0.09	0.07	0.18	0.06	0.10	0.08	*0.06*	0.16
Sn	1.33	0.53	1.73	1.44	2.35	1.17	1.75	1.72	1.26	*1.45*	1.76
Cs	0.22	0.16	0.32	0.21	0.22	b.d.l.	0.27	0.23	b.d.l.	*0.16*	0.68
Ba	257.7	201.5	291.2	271.0	175.2	236.0	289.6	288.9	230.8	*160.0*	257.8
La	42.1	33.3	44.1	42.7	24.2	30.6	43.0	39.6	36.0	*19.9*	41.5
Ce	87.3	78.8	97.7	89.3	55.9	60.3	89.4	81.0	78.2	*45.0*	83.0
Pr	9.96	9.75	12.25	10.06	7.07	7.44	10.31	9.86	9.81	*5.51*	10.70
Nd	40.6	42.8	42.5	40.9	31.6	32.0	40.0	37.1	36.2	*24.1*	37.8
Sm	7.00	8.56	8.06	6.56	7.02	7.70	7.71	7.57	9.17	*5.23*	8.26
Eu	1.87	2.73	2.51	2.45	2.28	2.29	2.28	2.09	1.92	*1.61*	2.18
Gd	5.84	6.22	6.57	5.54	6.33	7.58	6.00	4.36	6.98	*5.77*	3.75
Tb	0.83	1.39	0.96	0.93	0.89	0.93	0.83	0.70	0.79	*0.44*	1.07
Dy	4.40	5.06	5.19	5.03	6.08	4.39	4.75	4.77	4.83	*4.14*	3.86
Ho	0.98	1.00	0.76	0.94	1.05	1.00	0.90	0.49	1.00	*1.07*	0.93
Er	2.08	3.02	2.39	2.10	2.42	2.96	2.39	1.78	2.39	*3.06*	1.74
Tm	0.32	0.29	0.32	0.30	0.27	0.26	0.26	0.26	0.39	*0.28*	0.15
Yb	1.71	1.35	1.40	1.51	1.61	1.88	2.01	1.69	1.07	*2.03*	1.50
Lu	0.21	0.23	0.23	0.27	0.27	0.35	0.22	0.12	0.22	*0.14*	0.38
Hf	4.61	7.06	5.60	4.85	5.90	3.33	4.68	5.68	4.98	*3.06*	7.26
Ta	2.95	2.96	3.43	2.91	2.24	1.80	3.35	3.63	3.32	*2.15*	3.29
W	0.90	3.70	1.04	0.91	0.37	0.24	0.67	1.42	0.41	*0.27*	0.84
Tl	0.04	b.d.l.	0.03	0.04	b.d.l.	b.d.l.	0.04	b.d.l.	0.07	*b.d.l.*	b.d.l.

Pb	2.44	1.66	3.27	2.44	1.74	2.19	2.69	3.44	2.82	*1.52*	1.98
Th	4.22	3.30	4.73	4.42	2.34	2.68	4.43	4.15	4.20	*2.32*	4.04
U	1.26	0.88	1.33	1.37	0.70	0.73	1.28	1.22	1.14	*0.55*	0.95
T (°C) [b]	1172	1168	1177	1179	1185	1124	1225	1198	1208	*1180*	1195

Table 1 continued

Sample	u7gl107	u9gl73	u9gl76
Major elements (wt%)			
SiO2	48.1	50.1	49.5
TiO2	2.9	2.7	2.9
Al2O3	13.7	14.6	14.4
FeO	9.6	8.2	8.4
MnO	0.2	0.2	0.2
MgO	8.40	7.20	7.50
CaO	12.8	13.0	13.0
Na2O	2.9	3.0	2.9
K2O	1.2	0.8	0.9
P2O5	0.40	0.40	0.30
T (°C) [b]	1215	1216	1179

[a] Measurements are contaminated by small amounts of olivine, which affects Co and Ni. Other trace elements are not affected

[b] Temperature calculated from equilibrium conditions between olivine and melt inclusions.

- Debunscha Maar magmas mixed and fractional crystallised at upper mantle depths
- Its main magma source is peridotite with a minor pyroxenite component
- Amphibole signal and high olivine Ca/Al indicate a metasomatised peridotite mantle
- Mantle potential temperatures give no sign of an anomalous hot mantle